Appl. Phys. A (2014) 116:2077–2085
DOI 10.1007/s00339-014-8404-5

Applied Physics A
Materials Science & Processing

Structural characterization, magnetic properties and magnetocaloric effects of $La_{0.75}Sr_{0.25}Mn_{1-x}Cr_xO_3$ ($x = 0.15$, 0.20, and 0.25)

Ah. Dhahri · E. Dhahri · E. K. Hlil

Received: 31 October 2013 / Accepted: 24 March 2014 / Published online: 5 April 2014

Abstract The effect of Cr doping on the structural, magnetic and magnetocaloric properties of perovskite manganites $La_{0.75}Sr_{0.25}Mn_{1-x}Cr_xO_3$ ($x = 0.15$, 0.20, and 0.25) has been investigated. Crystalline structure and magnetic properties are investigated by using X-ray powder diffraction and magnetization measurements, respectively. All samples show a single phase and are found to crystallize in the distorted rhombohedral system with $R\bar{3}c$ space group. A monotonous change of Curie temperature (T_C), from 314 to 253 K, is observed when content doping increases. Substantial magnetic entropy change reaching 4.20 J/kg K is revealed. Relative cooling power was estimated as well. It was found to reach 289, 323, and 386 J/kg for $x = 0.15$, 0.20, and 0.25, respectively. Field dependence of the magnetic entropy change showing the power law dependence $\Delta S_M \propto (\mu_0 H)^n$ is also analyzed and discussed.

1 Introduction

Perovskite manganites with a chemical formula of $R_{1-x}A_xMnO_3$ (R: trivalent rare-earth cation, A: divalent alkaline earth cation) have been extensively investigated during the last two decades, thanks to their immediate technological applications. They show attractive physical properties such as giant magnetoresistance as well as magnetocaloric effect (MCE) [1]. From refrigeration point of view, the conventional refrigeration technologies based on the cycle of gas expansion/compressed cooling mechanisms are expected to be replaced by the environment friendly and more efficient magnetic refrigeration in near future [1, 2]. Magnetic refrigeration is based on the MCE. This latter results from a system coupling magnetic moments under the influence of an external magnetic field. It results in the cooling or heating of the system. Currently, the development of this technology is linked to research on materials presenting optimal magnetocaloric properties [namely, large magnetic entropy change (ΔS_M) and relative cooling power (RCP) at near room temperature]. Recently, an intensive interest in perovskite-type manganese oxides $Re_{1-x}M_xMnO_3$ (Re: rare-earth ions such as La^{3+}, Pr^{3+} , and Nd^{3+}…, M: divalent alkaline earth ion such as Ca^{2+}, Sr^{2+}, Ba^{2+}…) has been prompted by the observation of substantial magnetocaloric effect. Among these, perovskite manganites are of special interest, as they are known to tune magnetocaloric properties such as the transition temperature, magnetic density as well as the coercive magnetic field. Such magnetic parameters are very sensitive to the substitution of Mn by other 3d elements, because this substitution causes the change of ratio of amount Mn^{3+}/Mn^{4+} in these manganites [3]. In addition, the magnetic properties of the manganites' phases are strongly affected by the Mn–O bond length and Mn–O–Mn bond angle that are controlled by the ionic radii of Re, Mn site ions and Mn^{3+}/Mn^{4+} ratio, which modifies the double-exchange (DE) and super-exchange (SE) interactions [4, 5]. The magnetic and transport properties of these systems are then determined by the competition between DE and SE. In manganites, it is possible to dope at both Re and Mn sites. Moreover, Re-

Ah. Dhahri (✉) · E. Dhahri
Laboratoire de Physique Appliquée, Faculté des Sciences de Sfax, Université de Sfax, BP 1171, 3000 Sfax, Tunisia
e-mail: dhahri.ahmad@gmail.com

E. K. Hlil
Institut Néel, CNRS et Université Joseph Fourier, BP 166, 38042 Grenoble, France

site doping is known to control the Mn^{3+}/Mn^{4+} ratio in the material. Compared with Re-site doping, Mn-site doping is more important because it does not only modify the Mn^{3+}–O^{2-}–Mn^{4+} network but also brings the doped transition metal ions. From a fundamental point of view, universal curve for the magnetic entropy change for second-order transition materials has recently been reported [6]. It can be constructed using a phenomenological procedure, which does not require the knowledge of either the equation of state or the critical exponents of the material. In order to establish a relationship between the exponent (n) and the critical exponents of the material, field dependence of entropy change (follows a power law $\Delta S_M \propto (\mu_0 H)^n$) and relative cooling power are checked [7, 8].

In this paper, a detailed investigation is carried out on magnetocaloric effect, field dependence on MCE and critical behavior in $La_{0.75}Sr_{0.25}Mn_{1-x}Cr_xO_3$ ($x = 0.15$, 0.20, and 0.25) system. The universality of magnetic entropy change for the compounds is also investigated and discussed.

2 Experimental

$La^{3+}_{0.75}Sr^{2+}_{0.25}Mn^{3+}_{0.75-x}Cr^{3+}_{x}Mn^{4+}_{0.25}O^{2-}_{3}$ (LSMCr$_x$) ($x = 0.15$, 0.20, and 0.25) polycrystalline samples were prepared by solid-state reaction method. The powders mixed in the stoichiometric composition of dried high-purity La_2O_3, $SrCO_3$, MnO_2, and Cr_2O_3 were ground and calcined at 1,173 K for 24 h in air for several times with intermediate grinding to ensure homogenization. The powders were pressed into pellet forms under 4 ton/cm^2 and sintered at 1,673 K for 24 h in air with several periods of grinding and repelletizing. Finally, these pellets were quenched at room temperature. This step was carried out to conserve the structure at an annealed temperature. The structure and phase purity were checked by powder X-ray diffraction (XRD) using CuKα radiation ($\lambda = 1.5406$ Å) at room temperature. The patterns were recorded in the $20° \leq 2\theta \leq 86°$ angular range with a step of 0.017° and counting time of 18 s per step. According to our measurements, this system can detect up to a minimum of 3 % of impurities. Structural analysis was carried out with the Rietveld structural refinement program using FULLPROF software (Version 1.9c-May 2001-LLB-JRC) [9].The microstructure was observed by scanning electron microscope (SEM) using a Philips XL30, and a semi-quantitative analysis was performed at 15-kV accelerating voltage using energy dispersive X-ray analyses (EDX).

Magnetization measurements versus both temperature and magnetic field (μ_0H) curves were carried out using BS1 and BS2 magnetometer developed in Louis Neel Laboratory of Grenoble.

3 Results and discussion

3.1 Scanning electron microscope

The morphology and particle size of LSMCr$_x$ samples ($x = 0.15$ and 0.25) are shown in the inset of Fig. 1. These micrographs show that the introduction of Cr^{3+} ions strongly reduces the grain size which decreases from 197 to 113 nm for $x = 0.15$ and 0.25, respectively. However, we can also calculate the average grain size (S) from the XRD peaks using the Scherrer formula:

$$S = \frac{0.9\,\lambda}{\beta\,\cos\theta} \quad (1)$$

Where λ is the used X-ray wavelength, θ the diffraction angle for the most intense peak (1 0 4), and $\beta$is defined as $\beta^2 = \beta_m^2 - \beta_s^2$. Here, β_m is the experimental full width at half maximum (FWHM) and β_s is the FWHM of a standard silicon sample [10]. The obtained values for (S) are 66 and 38 nm for the samples with $x = 0.15$ and 0.25, respectively. Obviously, the particle sizes observed by SEM are several times larger than those calculated by XRD, which indicates that each particle observed by SEM consists of several crystallized grains.

3.2 X-ray analysis

All LSMCr$_x$ ($x = 0.15$, 0.20, and 0.25) samples are in a single phase. The diffraction peaks are sharp and can be indexed on rhombohedra structure with the $R\bar{3}c$ space group, hexagonal setting ($Z = 6$), in which the La/Sr atoms are at 6a (0, 0, ¼), Mn/Cr at 6b (0, 0, 0) and O at 18e (x, 0, ¼) positions. No traces of secondary phases were detected within the sensitivity limits of the experiment (a few percent). Figure 1 shows an example of the Rietveld refined X-ray diffraction pattern of LSMCr$_{0.2}$. The difference between the experimental and calculated intensities is given at the bottom of the plot. The refinement quality factors (R_{wp}, R_P, R_F and χ^2) are satisfactory as reported in Table 1. With increasing Cr concentration, the lattice parameters change in a continuous manner indicating perfect solid solubility of Cr at Mn site. A decrease in the lattice volume with an increase in Cr content from $x = 0.15$ to 0.25 can be explained by the replacement of Mn^{3+} ions ($r_{Mn^{3+}} = 0.65$ Å) by a smaller Cr^{3+} ions ($r_{Cr^{3+}} = 0.615$ Å) [11]. This hypothesis was confirmed by the determination, from the Rietveld refinement, of (Mn/Cr)–O distance calculated from the structural parameters (see Table 2). On the basis of refined crystallographic data, the unit cell, atomic parameters and other fitting parameters of all the samples are computed and are gathered in Table 1.

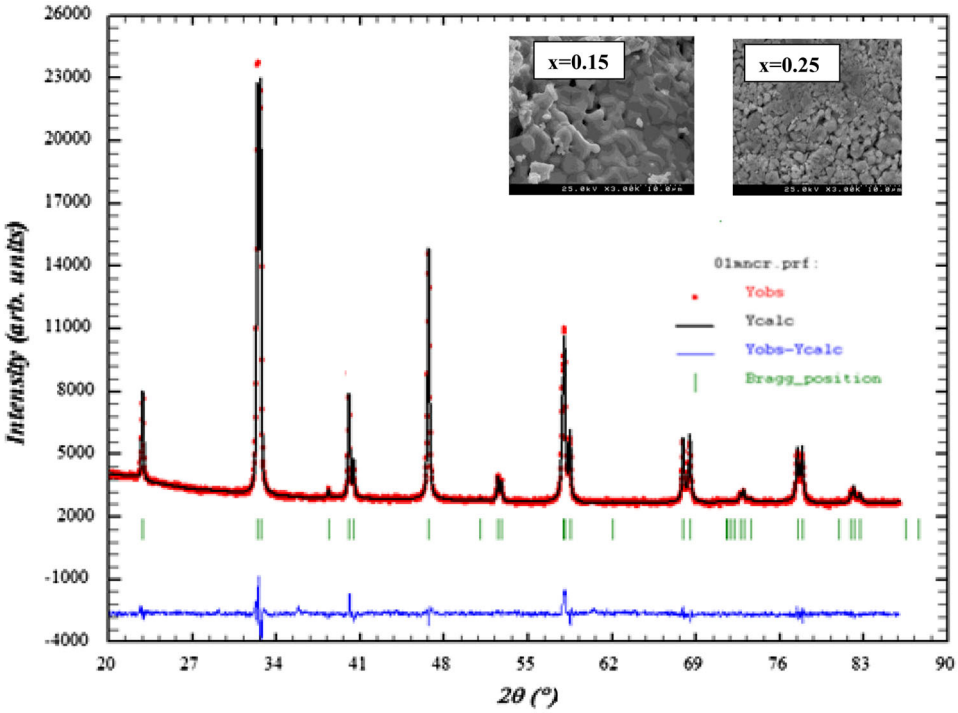

Fig. 1 Observed (*open symbols*) and calculated (*solid lines*) X-ray diffraction pattern for $La_{0.75}Sr_{0.25}Mn_{0.8}Cr_{0.2}O_3$ sample. Position for the Bragg reflection is marked by *vertical bars*. Differences between the observed and the calculated intensities are shown at the *bottom* of the diagram. *Inset* shows scanning electron micrographs of $La_{0.75}Sr_{0.25}Mn_{1-x}Cr_xO_3$ ($x = 0.15$ and 0.25) samples showing transect surface morphology of pellets prepared in the same condition

Table 1 Refined structural parameters from X-ray powder diffraction data for $La_{0.75}Sr_{0.25}Mn_{1-x}Cr_xO_3$ compounds having $R\bar{3}c$ space-group symmetry. Numbers in parentheses are statistical errors of the last significant digit

x	0.15	0.20	0.25
$R\bar{3}c$ phase			
a (Å)	5.51444 (6)	5.5122 (4)	5.5111 (3)
c (Å)	13.3676 (9)	13.3574 (7)	13.3554 (2)
V (Å^3)	352.02 (6)	351.48 (9)	351.28 (8)
(La/Sr) (6a) B_{iso} (Å^2)	0.47 (3)	0.33 (2)	0.53 (6)
(Mn/Cr) (6b) B_{iso} (Å^2)	0.23 (4)	0.18 (8)	0.22 (4)
(O) (18e) B_{iso} (Å^2)	0.2 (5)	0.73 (8)	0.35 (5)
x (O)	0.447 (8)	0.442 (3)	0.439 (2)
Discrepancy factors			
R_{wp} (%)	3.24	3.1	4.3
R_p (%)	2.3	2.3	2.9
R_F (%)	6.4	6.53	6.3
χ^2 (%)	2.14	1.43	2.12

Weight fraction resulting from the Rietveld analysis is expressed in percent of $La_{0.75}Sr_{0.25}Mn_{1-x}Cr_xO_3$. a and c hexagonal cell parameters, V cell volume, B_{iso} isotropic thermal parameter, x oxygen position, R_{wp}, R_p, *and* R_F the residuals for, respectively, the weighted pattern, the pattern and the Bragg structure factor

The tolerance factor is defined as:

$$t = \left(\frac{\langle r_A \rangle + r_o}{\sqrt{2}(\langle r_B \rangle + r_o)} \right) \quad (2)$$

Table 2 Values of average distance and angle in $La_{0.75}Sr_{0.25}Mn_{1-x}Cr_xO_3$ ($x = 0.15$, 0.20 and 0.25) compounds

X	0.15	0.20	0.25
$d_{(Mn/Cr)-O}$ (Å)	1.959 (8)	1.961 (1)	1.966 (5)
$\theta_{(Mn/Cr)-O-(Mn/Cr)}$ (°)	167.37 (6)	166.19 (1)	163.58 (2)
$<r_B>$ (Å)	0.615	0.613	0.611
T	0.947	0.948	0.949
W (u.a) $\times 10^{-2}$	9.445	9.401	9.289

Where $\langle r_A \rangle$, $\langle r_B \rangle$ and r_O are the average ionic radii of A, B, and O perovskite sites (ABO_3), respectively. As t value is close to 1, perovskite structure is expected to have a cubic form. The rhombohedral distortion may be viewed as a rotation of the octahedra around the threefold axis by an angle ω from the ideal perovskite position. This rotation describes the buckling of the MnO_6 octahedra caused by the ionic radii mismatch between A and B cations. The rotation angle (ω) can be calculated from the oxygen position (x) using the following relation [12]:

$$\omega = \arctan\left(\sqrt{3} - x\sqrt{12}\right) \quad (3)$$

The obtained values are 10.40, 11.36, and 11.93 for $x = 0.15$, 0.20, and 0.25, respectively. They indicate large distortions for all the compositions. For regular Mn coordination octahedra, the relation between ω and super-exchange (Mn/Cr)–O–(Mn/Cr) bond angle (θ) is given by [13]:

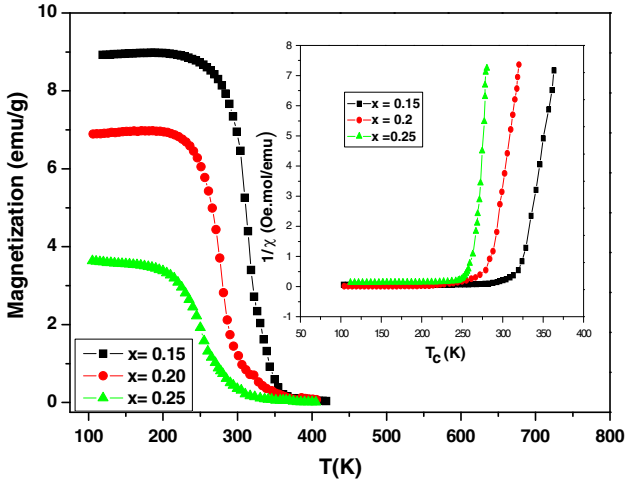

Fig. 2 Temperature dependence of the magnetization for $La_{0.75}Sr_{0.25}Mn_{1-x}Cr_xO_3$ ($x = 0.15$, 0.20 and 0.25) samples at $\mu_0 H = 0.05$ T magnetic field. The *inset* shows the inverse susceptibility versus temperature of $La_{0.75}Sr_{0.25}Mn_{1-x}Cr_xO_3$($x = 0.15$, 0.20 and 0.25) compounds obtained from magnetization measurement in a magnetic field of 0.05 T

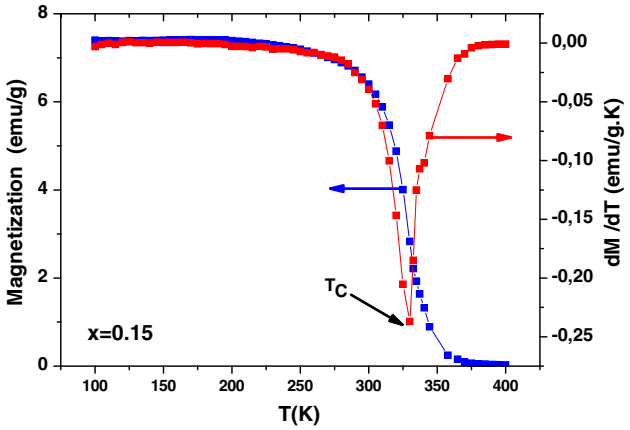

Fig. 3 The derivative of magnetization vs. T plots for $x = 0.15$

$$\cos\,\theta\,=\,\frac{(1\,-\,4\cos^2\omega)}{3} \tag{4}$$

Using ω values, we have calculated the θ values that are found to be in reasonable agreement with those obtained from Rietveld refinement (Table 2). The departure from 180° of (Mn/Cr)–O–(Mn/Cr) angle is a measure of the distortion. The bond length $d_{(Mn/Cr)-O}$ and bond angle $\theta_{(Mn/Cr)-O-(Mn/Cr)}$ variations have opposite effects on the unit cell volume (V). For a distorted perovskite, they are related by [14]:

$$V\,=\,Z\,[2d_{(Mn/Cr)-O}\,\cos\omega]^3 \tag{5}$$

with

$$\omega\,=\,\left[\frac{\pi\,-\,\theta_{(Mn/Cr)-O-(Mn/Cr)}}{2}\right] \tag{6}$$

and Z is the number of formula units in the unit cell ($Z = 6$ in the present case). The functional dependence of volume as a function of Cr concentration (x) is reproduced using the observed values of $d_{(Mn/Cr)-O}$ and $\theta_{(Mn/Cr)-O-(Mn/Cr)}$ in the above expression.

3.3 Magnetic characterizations

Figure 2 shows the temperature dependence of magnetization in field-cooled mode ($\mu_0 H\,=\,0.05\,T$) and reveals the presence of a sharp transition from a ferromagnetic to paramagnetic phase (FM–PM) for all $LSMCr_x$ ($x = 0.15$, 0.20 and 0.25) compounds. From this figure, we can clearly see that the introduction of the Cr ions diminishes considerably the magnetization. The same behavior was observed for Curie temperature (T_C), defined as the peak of dM/dT in the M–T curves (Fig. 3). A decrease of the T_C value is observed. It is equal to 317, 278, and 253 K for $x = 0.15$, 0.20, and 0.25, respectively.

Magnetization and T_C decrease can be related to two parameters. The first one is directly in relation with the mechanism of the double-exchange and super-exchange interactions in $La^{3+}_{0.75}Sr^{2+}_{0.25}Mn^{3+}_{0.75-x}Cr^{3+}_{x}Mn^{4+}_{0.25}O^{2-}_{3}$ compounds between Mn and Cr ions. The second parameter is associated to bandwidth (W) describing the overlap between Mn-3d and O-2p orbitals given by the following empirical formula [14]:

$$W\,\propto\,\frac{\cos[1/2(\pi\,-\,\gamma)]}{d^{3.5}_{(Mn/Cr)-O}} \tag{7}$$

As shown, this second parameter is in relation with the structure of the compounds, where γ is the (Mn/Cr)–O–(Mn/Cr) angle and $d_{(Mn/Cr)-O}$ is the bond length.

The estimated W values (Table 2; Fig. 4) indicate a decrease in bandwidth (W) when increasing the Cr concentration x. This decrease reduces the overlap between the O-2p and Mn-3d orbital, which in turn decreases the exchange coupling of Mn^{3+} to Mn^{4+} and Mn^{3+}–Cr^{3+}, resulting in a decrease of the magnetic ordering temperature T_C. Moreover, the decrease in T_C is mainly attributed to the decrease of the B–O–B bond angle.

The temperature dependence of the inverse magnetic susceptibility ($1/\chi$) is shown in the inset of Fig. 2 for $x = 0.15$, 0.20, and 0.25 samples. In the paramagnetic region, the relation between χ and the temperature T should follow Curie–Weiss law:

$$\chi\,=\,\frac{C}{T\,-\,\theta_P} \tag{8}$$

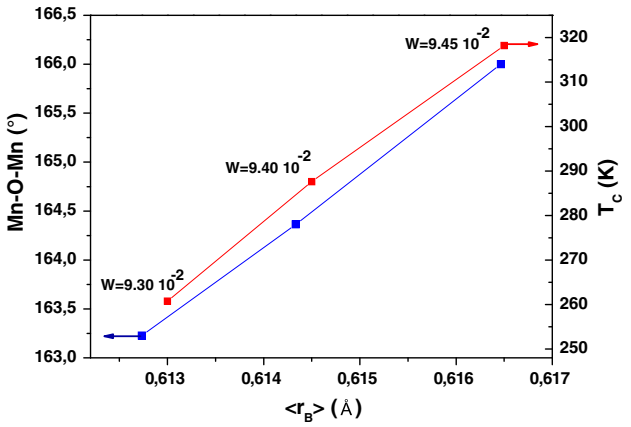

Fig. 4 Variation of bond angle (Mn/Cr)–O–(Mn/Cr) and T_C as function of the average ionic radii of B-site $<r_B>$ for $La_{0.75}Sr_{0.25}Mn_{1-x}Cr_xO_3$ ($x = 0.15$, 0.20 and 0.25) compounds

Table 3 Transition temperature T_C, Curie–Weiss temperature θ_p, experimental μ_{eff}^{exp} and calculated μ_{eff}^{theo} as function of Cr content for $La_{0.75}Sr_{0.25}Mn_{1-x}Cr_xO_3$ ($x = 0.15$, 0.20 and 0.25) compounds

Composition	T_C (K)	$\mu_{eff}^{theo}(\mu_B)$	$\mu_{eff}^{exp}(\mu_B)$	θ_P (K)
$La_{0.75}Sr_{0.25}Mn_{0.85}Cr_{0.15}O_3$	317	4.54	3.98	308
$La_{0.75}Sr_{0.25}Mn_{0.80}Cr_{0.20}O_3$	278	4.41	3.83	274
$La_{0.75}Sr_{0.25}Mn_{0.75}Cr_{0.25}O_3$	253	4.28	3.83	257

Where C is Curie constant and, θ_p is Weiss temperature determined from the linear fit of the paramagnetic region (Table 3). The positive θ_p value indicates the presence of ferromagnetic interaction between spin. On the other hand, the C constant is related to the effective paramagnetic moment via the following relation [15]:

$$C = \left(\frac{N_A \mu_B^2}{3 k_B}\right) \mu_{eff}^2 \tag{9}$$

Where $N_A = 6.023 \times 10^{23}$ mol^{-1} is the number of Avogadro, $\mu_B = 9.27 \times 10^{-21}$ emu is the Bohr magneton, and $k_B = 1.38016 \times 10^{-16}$ erg K^{-1}is the Boltzmann constant. From the determined C parameter, we have deduced the μ_{eff}^{exp} values (Table 3) that are compared to those determined theoretically (μ_{eff}^{theo}) from the following equation:

$$\mu_{eff}^{theo} = \sqrt{(0.75 - x)\mu_{eff}^2(Mn^{3+}) + 0.25\,\mu_{eff}^2(Mn^{4+}) + x\,\mu_{eff}^2(Cr^{3+})} \tag{10}$$

Where $\mu_{eff}(Mn^{3+}) = 4.9\,\mu_B$ and $\mu_{eff}(Mn^{4+}) = 3.87\,\mu_B$ [16].

The $\mu_{eff}(Cr^{3+})$ is given by the following equation: $\mu_{eff}^{theo} = g\sqrt{J(J+1)}$ where $g = 1 + \frac{J(J+1)+S(S+1)-L(L+1)}{2J(J+1)}$ is the Landau factor, $J = |L - S|$ is the total moment, $L = \sum m_l$ is the orbital moment and $S = \sum m_S$ is the spin moment. For Cr^{3+}, $J = 3/2$ and $g_J = 2/5$ (as $S = 3/2$, $L = 3$) therefore $\mu_{eff}(Cr^{3+}) = 0.775\,\mu_B$.

As seen in Table 3, we can notice that the measured effective magnetic moments μ_{eff}^{theo} in the paramagnetic (PM) regime are significantly larger than the calculated ones. Terashita et al. [17] has explained this difference by the short-range ferromagnetic correlation in the PM state.

The Banerjee criterion has been frequently used to check the nature of the magnetic phase transition in manganites [18]. According to this criterion, the positive or negative slope of $\frac{\mu_0 H}{M}$ versus M^2 (Arrott plot) curves indicates whether the magnetic phase transition is of a second or a first order. The main panel of Fig. 5 shows that near the FM–PM transition phase, $\frac{\mu_0 H}{M}$versus M^2 curves clearly exhibit a positive slope in the entire M^2 range, which confirms that the transition is of a second order. According to the mean field theory, near the transition point, $\frac{\mu_0 H}{M}$versus M^2 should show a series of parallel lines at various temperatures and the line related to T_C should pass through the origin [19]. For example, the Arrott plot curves for $LSMCr_{0.2}$ ($x = 0.2$) sample are not linear, which indicates that the mean field theory is not valid. The deviation from mean field reveals the presence of inhomogeneous magnetic state of the samples. It is well known that in manganites inhomogeneous magnetic states are due to the phase separation phenomenon or to B-site disorder-induced competition between DE and SE interaction or to change in correlation range of the magnetic fluctuations from cation deficiency [20].

According to the classical thermodynamic theory, the magnetic entropy change $|\Delta S_M|$ induced by the variation of the external magnetic field from 0 to $\mu_0 H_{Max}$ is given by:

$$\Delta S_M(T, \mu_0 H) = S_M(T, \mu_0 H) - S_M(T, 0) = \int_0^{\mu_0 H_{Max}} \left(\frac{\partial S}{\partial H}\right)_T \mu_0 dH \tag{11}$$

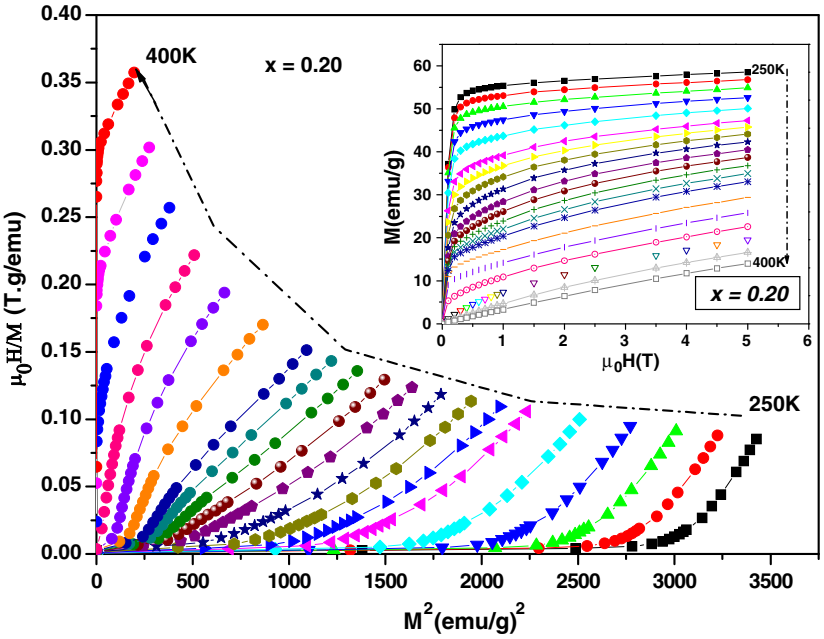

Fig. 5 Arrott plot of $\mu_0 H/M$ against M^2 at different temperatures. *Inset* shows the initial magnetization curves vs. magnetic field at different temperatures around T_C

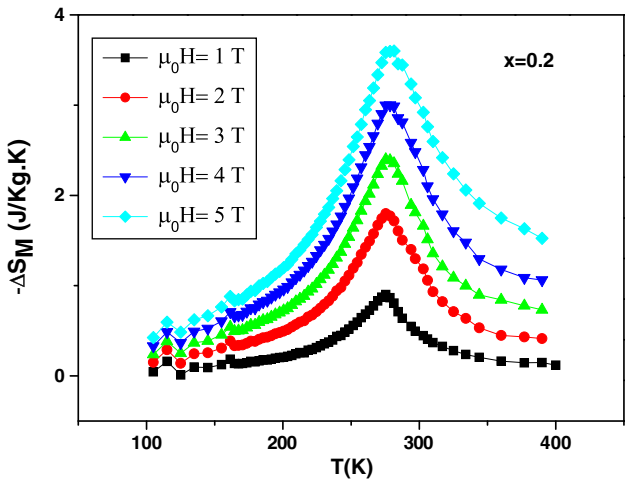

Fig. 6 Isothermal magnetic entropy change around the Curie temperature for polycrystalline $La_{0.75}Sr_{0.25}Mn_{0.80}Cr_{0.2}O_3$ sample

With Maxwell's thermodynamic relationship:

$$\left(\frac{\partial S_M(T,\mu_0 H)}{\partial M}\right)_T = \left(\frac{\partial M(T,\mu_0 H)}{\partial T}\right)_H \tag{12}$$

Equation (11) can be rewritten as follows:

$$\Delta S_M(T,\mu_0 \Delta H) = \int_0^{\mu_0 H_{\mathrm{Max}}} \left(\frac{\partial M(T,\mu_0 H)}{\partial T}\right)_H \mu_0 dH \tag{13}$$

Experimentally, two kinds of different methods are often used to evaluate the magnetic entropy change ΔS_M. The first one is the measurement of the M–T curve under different applied magnetic fields. The second one is the measurement of the M–$\mu_0 H$ curve under different temperatures. In this paper, we use the second method to calculate magnetic entropy change.

In order to evaluate the MCE, the changes of magnetic entropy (ΔS_M) curves can be numerically calculated using Eq. (14):

$$\Delta S_M\left(\frac{T_1,T_2}{2}\right) = \left(\frac{1}{T_2-T_1}\right)\left[\int_0^{\mu_0 H_{\mathrm{Max}}} M(T_2,\mu_0 H)\mu_0 dH - \int_0^{\mu_0 H_{\mathrm{Max}}} M(T_1,\mu_0 H)\mu_0 dH\right] \tag{14}$$

As shown in the inset of Fig. 5, the isothermal magnetizations versus applied field were measured at various temperatures for the $LSMCr_{0.2}$ sample. The magnetic entropy changes as a function of temperature of several external magnetic fields were calculated and plotted in Fig. 6. The values of $(-\Delta S_M)$ increase with the increase of the applied magnetic field. The peak of $(-\Delta S_M)$ versus T curve decreases with the increase of Cr substitution. For $\mu_0 H = 5\,T$, $(-\Delta S_M^{\max})$ reaches the value of 3.5 J/kg K at 317 K, 3.85 J/kg K at 278 K, and 4.20 J/kg K at 253 K for

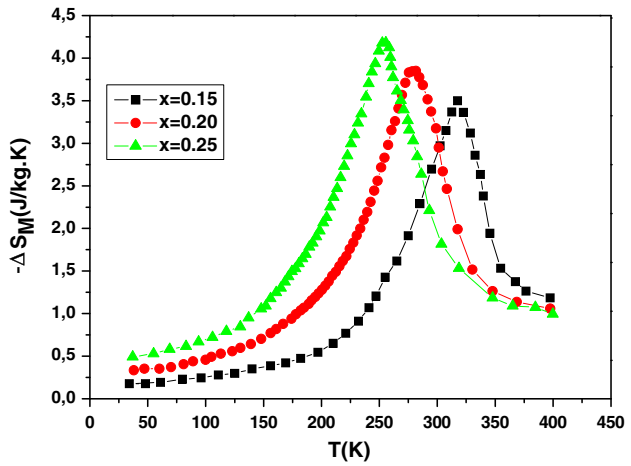

Fig. 7 Temperature dependence of the magnetic entropy change corresponding to an applied field $\mu_0 H = 5$ T of $La_{0.75}Sr_{0.25}Mn_{1-x}Cr_xO_3$ ($x = 0.15$, 0.2, and 0.25) compounds

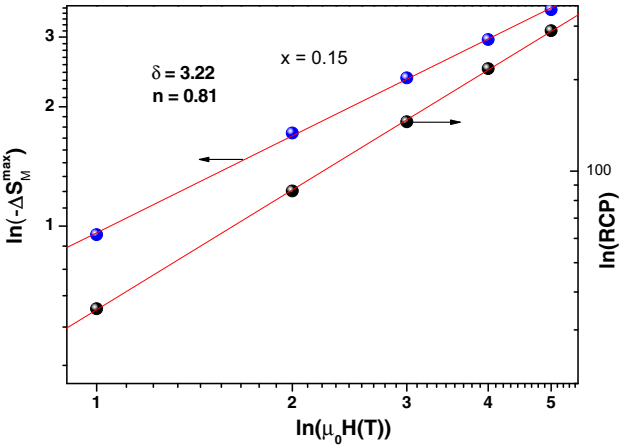

Fig. 8 Variation of $\ln(-\Delta S_M^{Max})$ and (RCP) as function of applied magnetic field for $La_{0.75}Sr_{0.25}Mn_{0.85}Cr_{0.15}O_3$ sample. *Red line* indicates the linear fit for n and δ calculation

Table 4 Summary of magnetocaloric properties of $La_{0.75}Sr_{0.25}Mn_{1-x}Cr_xO_3$ compared with other magnetic materials at $\mu_0 H = 5$T

Sample	T_C (K)	$\lvert\Delta S_m^{max}\rvert$(J/kg K)	RCP (J/K)	References
Gd	293	9.5	410	[27]
$La_{0.67}Ba_{0.33}MnO_3$	292	1.48	161	[4]
$La_{0.7}Sr_{0.3}Mn_{0.93}Fe_{0.07}O_3$	296	4	255	[28]
$La_{0.7}Sr_{0.3}Mn_{0.9}Al_{0.1}O_3$	310	2.6	109	[29]
Gd_5 (Si_2Ge_2)	275	18.5	535	[30]
$La_{0.75}Sr_{0.25}Mn_{0.85}Cr_{0.15}O_3$	317	3.5	289	This work
$La_{0.75}Sr_{0.25}Mn_{0.80}Cr_{0.20}O_3$	278	3.85	323	This work
$La_{0.75}Sr_{0.25}Mn_{0.75}Cr_{0.25}O_3$	253	4.2	386	This work

$x = 0.15$, 0.20, and 0.25, respectively (Fig. 7). To evaluate the applicability of ($LSMCr_x$) composition as a magnetic refrigerant, the obtained values of magnetic entropy change in our study are compared with other magnetic materials (Table 4).

According to Oesterreicher and Paker [21], the field dependence of the magnetic entropy change of materials with a second-order phase transition can be expressed as:

$$\Delta S_M \propto (\mu_0 H)^n \tag{15}$$

Where n depends on the magnetic state of the compound. On the basis of mean field approach, field dependence of magnetic entropy change at Curie temperature has been predicted to correspond to $n = 2/3$. The exponent n, dependent on $\mu_0 H$ and T, can be calculated as follows:

$$n = \frac{d\ \ln|\Delta S_M|}{d\ \ln(\mu_0 H)} \tag{16}$$

In the particular case of $T = T_C$ or at the temperature when the entropy is maximal, the exponent (n) becomes an independent field [22]. In this case,

$$n\,(T_C) = 1 + \frac{\beta - 1}{\beta + \gamma} \tag{17}$$

Where β and γ are the critical exponents [23].

With, $\beta\delta = (\beta+\gamma)$ [24], the relation (17) can be written as:

$$n\,(T_C) = 1 + \frac{1}{\delta}\left(1 - \frac{1}{\beta}\right) \tag{18}$$

To determine the exponent n, a linear plot of $(-\Delta S_M^{max})$ versus $\mu_0 H$ is constructed at the transition temperature of the peak of the magnetic entropy change, i.e., at 317 K for $LSMCr_{0.15}$, at 278 K for $LSMCr_{0.20}$ and at 253 K for $LSMCr_{0.25}$, (Fig. 8 as example for $x = 0.15$). The n values obtained from the slope are 0.88 ± 0.05, 0.80 ± 0.01, and 0.87 ± 0.01 for $x = 0.15$, 0.20, and 0.25, respectively. These values are higher than the mean field prediction ($n = 2/3$). This deviation is due to the presence of local homogeneities in the vicinity of transition temperature [25]. The change of specific heat associated with a magnetic field variation from zero to $\mu_0 H$is also computed using the following relationship [26]:

$$\begin{aligned}\Delta C_P(T, \mu_0 H) &= C_P(T, \mu_0 H) - C_P(T, 0) \\ &= T\frac{\partial(\Delta S_M(T, H))}{\partial T}\end{aligned} \tag{19}$$

Figure 9 shows the temperature dependence of ΔC_P under different field variations for $LSMCr_{0.2}$ sample calculated from the ΔS_M data (Fig. 7) using relation (19). The ΔC_P undergoes a sudden change from positive to negative around T_C with a positive value above T_C and a negative

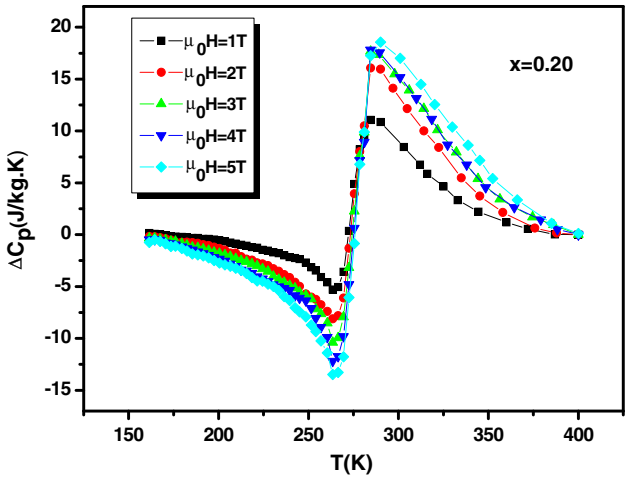

Fig. 9 Change of specific heat of the sample ($x = 0.20$) as a function of temperature at different magnetic field

one below T_C. The maximum/minimum value of ΔC_P, observed at 304/322 K for $x = 0.15$, 264/292 K for $x = 0.2$, and 242/257 K for $x = 0.25$ exhibits an increasing trend with applied field and is found to be equal to 16.70–12.02, 18.78–13.58, and 19.20–13.76 $Jkg^{-1}K^{-1}$ for $x = 0.15$, 0.20, and 0.25, respectively, at an applied field of 5 T.

Another useful parameter, which decides the efficiency of a magnetocaloric material, is the relative cooling power: RCP. It is the heat transfer between the hot and the cold tanks during an ideal refrigeration cycle. This represents numerically the area under $(-\Delta S_M)$ vs. T curve:

$$\mathrm{RCP} = -\Delta S_M(T, \mu_0 H) \times \partial T_{\mathrm{FWHM}} \tag{20}$$

Where $(\partial T_{\mathrm{FWHM}} = T_{\mathrm{hot}} - T_{\mathrm{cold}})$ is the full width at the maximum of the magnetic entropy change curve, and $\Delta S_M(T, \mu_0 H)$ is the maximum magnetic entropy change. For the Cr-doped samples, the estimated RCP values are found to range between 289 J/kg ($x = 0.15$) and 386 J/kg ($x = 0.25$).

Generally, the double-exchange interaction controls the close relationship between the structure and the magnetic properties in this type of material. When the rate of substituted Cr^{3+} ions increases, the antiferromagnetic coupling between Cr^{3+}–Cr^{3+}, Cr^{3+}–Mn^{4+} and Mn^{4+}–Mn^{4+} should be taken into consideration. In accordance with the work of Goodenough et al. [31], we expect a weak antiferromagnetic super-exchange interaction between two ions having an empty orbital; e.g., the partial substitution of Mn^{3+} by Cr^{3+} causes a decrease in the number of Mn^{3+}. In addition, the ferromagnetic double-exchange interactions between Mn^{4+} and Mn^{3+} ions are weakened, while the antiferromagnetic interactions between Mn^{4+} and Cr^{3+} are reinforced. Therefore, the partial replacement of Mn^{3+} by Cr^{3+} can greatly weaken the double-exchange interaction of Mn^{3+}–O–Mn^{4+} and, therefore, the full width at half maximum (FWHM) increases, which leads to an improvement of RCP.

Refrigerants with a wide working temperature span and a high RCP are in fact very beneficial to magnetic cooling applications. It is worth mentioning that while T_C is largely suppressed, the Cr substitution slightly affects the magnetic cooling effect.

The field dependence of RCP can be expressed as a power law:

$$\mathrm{RCP} \propto (\mu_0 H)^{1+1/\delta} \tag{21}$$

Where δ is the critical exponent of the magnetic transition. Field dependence of RCP is displayed in Fig. 8 for $x = 0.15$. The obtained values of δ are 3.2 (3), 3.34 (2), and 2.82 (4) for $x = 0.15$, 0.20, and 0.25, respectively. From the values of n and δ, the critical parameters β and γ are deduced for each compound using Eqs. (17) and (18) (Table 5).

The obtained values for all compounds show a slight deviation from the mean field model (Table 5) [32]. It is established that, the critical behavior of manganites is complex due to their intrinsic heterogeneity, the coexistence of multiphase and the non belonging of the critical exponents to any universality class [33, 34].

4 Conclusion

A detailed investigation of structural, magnetic, and magnetocaloric properties of polycrystalline $La_{0.75}Sr_{0.25}Mn_{1-x}Cr_xO_3$ ($x = 0.15$, 0.20 and 0.25) compounds is reported. All samples are found to crystallize in a rhombohedral structure with $R\bar{3}c$ space group, and a volume decrease is observed when Cr content increases. From magnetic investigations, Arrott plots reveal the presence of a second-

Table 5 Critical β and γ parameters calculated from nand δ

Composition	References	T_C (K)	N	δ	β	γ
$La_{0.75}Sr_{0.25}Mn_{0.85}Cr_{0.15}O_3$	This work	317	0.88 (5)	3.22 (3)	0.714	1.585
$La_{0.75}Sr_{0.25}Mn_{0.80}Cr_{0.20}O_3$	This work	278	0.80 (1)	3.34 (2)	0.600	1.404
$La_{0.75}Sr_{0.25}Mn_{0.75}Cr_{0.25}O_3$	This work	253	0.870 (1)	2.82 (4)	0.730	1.330
Mean field model	[32]		0.66	3	0.5	1

order magnetic transition in all three samples. The magnitude of MCE and the relative cooling power (RCP) are considerably improved when Cr content increases. Furthermore, Cr-doped manganites' compounds have many advantages. They are inexpensive, easy to synthesize, and chemically stable. This is because their Curie temperatures can be tailored between 253 and 317 K by adjusting the dopant (Cr) concentration. Based on our results, the $La_{0.75}Sr_{0.25}Mn_{1-x}Cr_xO_3$ system appears to be a good candidate for a multicomponent magnetic refrigerator over a wide temperature range.

References

1. S. Gama, A.A. Coelho, A. de Campos, A. Magnus, G. Carvalho, F.C.G. Gandra, Phys. Rev. Lett. **93**, 237202 (2004)
2. F.X. Hu, B.G. Shen, J.R. Sun, Z.H. Chen, G.H. Rao, X.X. Zhang, Appl. Phys. Lett. **78**, 3675 (2001)
3. K. Cherif, J. Dhahri, E. Dhahri, M. Oummezine, H. Vincent, J. Solid State Chem. **163**, 732 (2002)
4. D.T. Morelli, A.M. Mane, J.V. Mantese, A.L. Micheli, J. Appl. Phys. **79**, 373 (1996)
5. L.E. Hueso, P. Sande, D.R. Miguens, J. Rivas, F. Rivadulla, M.A. Lopez-Quintela, J. Appl. Phys **91**(12), 9943–9947 (2002)
6. R. Cabellero-Flores, V. Franco, A. Conde, L.F. Kiss, J. Appl. Phys. **108**, 073921 (2010)
7. V. Franco, A. Conde, D.S. Sidhaye, B.L.V. Prasad, P. Poddar, S. Srinath, M.H. Phan, H. Srikanth, J. Appl. Phys. **107**, 09A902 (2010)
8. M. Halder, S.M. Yusuf, M.D. Mukadam, K. Shashikala, Phys. Rev B **81**, 174402 (2010)
9. H.M. Rietveld, J. Appl. Crystallogr. **2**, 65 (1969)
10. A. Guinier, Théorie et Technique de la Radiocristallographie, Dunod, Paris 3rd ed (1964)
11. R.D. Shannon, Acta Crystallogr. Sect. A: Cryst. Phys. Diffr. Theor. General Crystallogr. **A32**, 751–767 (1976)
12. E. Rodriguez, I. Alvarez, M.L. Lopez, M.L. Veiga, C. Pico, J. Solid State Chem. **148**, 479 (1999)
13. M.O. Keeffe, B.G. Hyde, Acta Crystallogr. B **33**, 3802 (1977)
14. P.G. Radaelli, G. Iannone, M. Marezio, H.Y. Hwang, S.W. Cheong, J.D. Jorgensen, D.N. Argyriou, Phys. Rev. B. **56**, 8265 (1997)
15. C. B. JURCA, Synthèse et caractérisation de pérovskites doubles magnétorésistives dérivées de Sr_2FeMoO_6 thèse (2004)
16. B.D. Cullity, *Introduction to Magnetic Material* (Addison-Wesley, London, 1972)
17. H. Terashita, J.J. Neumeier, Phys. Rev. B **71**(134402), 225408 (2009)
18. L.E. Hueso, P. Sande, D.R. Miguéns, J. Rivas, F. Rivadulla, M.A. López-Quintela, J. Appl. Phys. **91**, 9943 (2002)
19. J. Mira, J. Rivas, F. Rivadulla, C. Vázquez, M.A. López-Quintela, Phys. Rev. **B60**, 2998 (1999)
20. P.H. Vanderbemden, B. Vertruyen, A. Rulmont, R. Clouts, G. Dhalenne, M. Ausloos, Phys. Rev. B **68**, 224418 (2003)
21. H. Oesterreicher, F.T. Paker, J. Appl. Phys. **55**, 4336 (1984)
22. V. Franco, A. Conde, M.D. Kuz'min, J.M. Romero-Enrique, J. Appl. Phys. **105**(7), 917–920 (2009)
23. V. Franco, A. Conde, Int. J. Refrig **33**, 465 (2010)
24. B. Widom, J. Chem. Phys. **43**, 3898 (1965)
25. Q.Y. Dong, H.W. Zhang, J.R. Sun, B.G. Shen, V. Franco, J. Appl. Phys. **103**, 116101 (2008)
26. A. Rostamnejadi, M. Venkatesan, P. Kameli, H. Salamati, J.M.D. Coey, J. Magn. Magn. Mater. **323**, 2214 (2011)
27. M.H. Phan, S.C. Yu, J. Magn. Magn. Mater. **308**, 325 (2007)
28. S.K. Barik, C. Krishnamoorthi, R. Mahendiran, J. Magn. Magn. Mater. **323**, 1015 (2011)
29. D.N.H. Nam, N.V. Dai, L.V. Hong, N.X. Phuc, S.C. Yu, M. Tachibana, E. Takayama-Muromachi, J. Appl. Phys. **103**, 043905 (2008)
30. V.H. Percharsky, K.A. Gschneider, A.O. Tsokol, Rep. Prog. Phys. **68**, 1479 (2005)
31. J.B. Goodenough, A. Wold, R.J. Arnott, N. Menyuk, Phys. Rev. **124**, 373 (1961)
32. S.J. Xu, W. Tong, J.Y. Fan, J. Gao, C. Zha, Y.H. Zhang, J. Magn. Magn. Mater. **288**, 92 (2005)
33. H.S. Shin, J.E. Lee, Y.S. Nam, H.L. Ju, C.W. Park, Solid State Commun. **118**, 377 (2001)
34. C.S. Hong, W.S. Kim, N.H. Hur, Phys. Rev. B **63**, 092504 (2001)